AD-A084 762 ACCUMETRICS CORP CAMBRIDGE MA F/G 14/2
APPLIED RESEARCH & DEVELOPMENT OF TRIAXIAL PIEZOELECTRIC (PZL) --ETC(U)
JUN 79 D H FRYKLUND F19628-77-C-0163
UNCLASSIFIED AFGL-TR-79-0101 NL

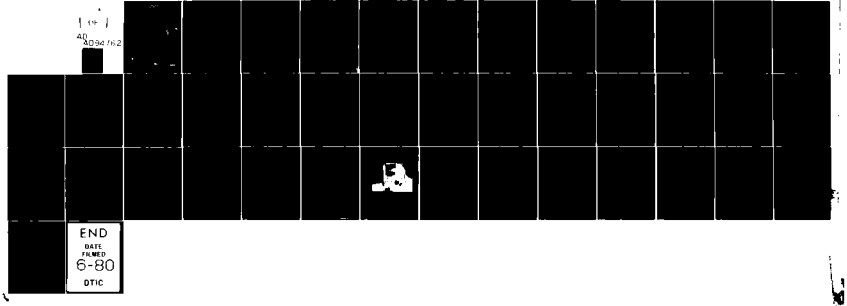

END
DATE FILMED
6-80
DTIC

LEVEL IV

12

AFGL-TR- 79-0101

AD A084762

# APPLIED RESEARCH & DEVELOPMENT OF TRIAXIAL PIEZOELECTRIC (PZL) ACCELEROMETER SYSTEMS OF IMPROVED DESIGN

Donald H. Fryklund

Accumetrics Corporation
344 Ringe Avenue
Cambridge, Massachusetts 02140



June 1979

Final Report for period 77 March to 79 June

Approved for Public Release; distribution unlimited



AIR FORCE GEOPHYSICS LABORATORY
AIR FORCE SYSTEMS COMMAND
UNITED STATES AIR FORCE
HANSCOM AFB, MASSACHUSETTS 01731

80 5 27 004

Unclassified

SECURITY CLASSIFICATION OF THIS PAGE (When Data Entered)

| REPORT DOCUMENTATION PAGE | READ INSTRUCTIONS BEFORE COMPLETING FORM |
|---|---|
| 1. REPORT NUMBER (19) AFGL-TR-79-0101 | 2. GOVT ACCESSION NO. AD-A084 762 |
| 4. TITLE (and Subtitle) APPLIED RESEARCH & DEVELOPMENT OF TRIAXIAL PIEZOELECTRIC (PZL) ACCELEROMETER SYSTEMS OF IMPROVED DESIGN, | 5. TYPE OF REPORT & PERIOD COVERED (9) Final Report, Mar 77 — Jun 79, |
| 7. AUTHOR(s) Donald H./Fryklund | 8. CONTRACT OR GRANT NUMBER(s) F19628-77-C-0163 |
| 9. PERFORMING ORGANIZATION NAME AND ADDRESS Accumetrics Corporation, 344 Ringe Avenue Cambridge, Massachusetts 02140 | 10. PROGRAM ELEMENT, PROJECT, TASK AREA & WORK UNIT NUMBERS 62101F SAMS00AB 669001AU |
| 11. CONTROLLING OFFICE NAME AND ADDRESS Air Force Geophysics Laboratory Hanscom AFB, Massachusetts 01731 Monitor/Andrew C. Faire/LKB | 12. REPORT DATE Jun 79 |
| | 13. NUMBER OF PAGES 46 |
| 14. MONITORING AGENCY NAME & ADDRESS (if different from Controlling Office) (16) AFGL, 6690 | 15. SECURITY CLASS. (of this report) Unclassified |
| | 15a. DECLASSIFICATION DOWNGRADING SCHEDULE |

16. DISTRIBUTION STATEMENT (of this Report)

Approved for public release; distribution unlimited

(17) 00, 02

17. DISTRIBUTION STATEMENT (of the abstract entered in Block 20, if different from Report)

18. SUPPLEMENTARY NOTES

19. KEY WORDS (Continue on reverse side if necessary and identify by block number)

Piezoelectric
Accelerometer
Densitometer
Transducer
Atmospheric density

20. ABSTRACT (Continue on reverse side if necessary and identify by block number)

Refinements in the accelerometer system used in the falling-sphere atmospheric density measuring system have been implemented. These include a redesigned Z-axis amplifier chain, range scale changes in the X and y axis amplifier ouputs to provide overlap, and a new temperature monitor circuit. The squib initiation circuit and squib holder bushing has been redesigned for greater reliability. Calibration has been improved by the use of a specially-designed function generator. Five systems were fabricated. Three systems were flown at Kwajalein, M.I. and Red Lake, Canada.

DD FORM 1 JAN 73 1473 EDITION OF 1 NOV 65 IS OBSOLETE

Unclassified 404122

SECURITY CLASSIFICATION OF THIS PAGE (When Data Entered)

# FOREWORD

This document is the final report required under AFGL Contract No. F19628-77-C-0163 describing the contract effort to evolve and fabricate improved falling sphere densitometer systems.

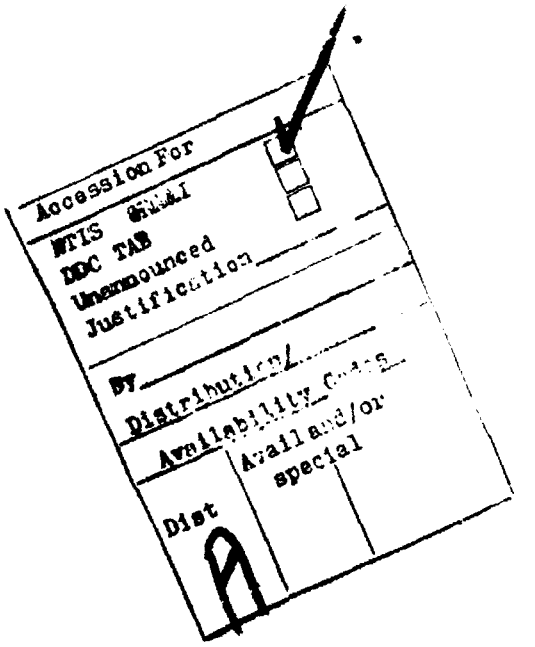

CONTENTS

## LIST OF FIGURES

## NOMENCLATURE

| | |
|---|---|
| a | Acceleration, instantaneous |
| A | Acceleration, peak or steady state |
| A | Constant |
| B | Constant |
| C | Capacitance, farads, microfarads |
| d | Distance |
| E | Emf, volts |
| F | Force |
| f | Frequency, Hz |
| $f_n$ | Natural frequency, Hz |
| g | Acceleration due to gravity |
| K | Spring constant |
| K | Constant of proportionality |
| K | Gain |
| L | Length |
| m | Mass |
| R | Resistance, ohms |
| R | Radius |
| r | Radius |
| t | Time, seconds |
| T | Tolerance |
| T | Time constant |
| V | Voltage, volts |
| $V_0$ | Voltage, output, volts |
| W | Energy |
| x | Distance, instantaneous |
| X | Distance, steady state |
| $\omega$ | Frequency, angular velocity, radians/second |
| $\omega_n$ | Natural angular frequency, zero-g |
| $\omega_{nT}$ | Natural angular frequency, Test, sea level |
| $\omega_{ns}$ | Natural angular frequency, Flight |
| $\omega_s$ | Spin angular frequency |

# I. INTRODUCTION

The object of the effort under this contract was to further refine the AFGL falling-sphere upper atmospheric density measuring system reported in Documents AFCRL-72-0033, AFCRL-TR-74-0123, AFGL-TR-76-0064, and AFGL-TR-77-0187, and to fabricate and provide field services for five falling-sphere systems. This effort involved postflight data analysis to obtain information leading to improvements in the flight system, and in the laboratory integration and calibration techniques.

Considerable effort was expended in refinements to improve the accuracy of calibration of the accelerometer. This included the redesign and fabrication of a new test bench and fixture for the calibration of the transducers, the evolvement of transducer natural frequency correction formulae to compensate for gravity and spin affects, and the design and fabrication of a special-purpose function generator to enable a more precise calibration of the Z-axis amplifiers.

Field services were provided for rocket programs at Kwajalein, M.I. where two systems were flown; at Red Lake, Ontario, Canada where one system was flown; and at WSMR, New Mexico where prelaunch preparations were made for one system but launch was cancelled due to a malfunction in the prime rocket (Aerobee 170) of the program.

## II. AMPLIFIER MODIFICATION AND CALIBRATION

### 2.0 General

The spin modulation of the air drag acceleration enables the use of a.c. amplifiers to process the transducer output to provide acceptable levels for telemetering. Thus, the amplifier can be tuned to the spin frequency and can be designed to reject interfering signals, noise, and low frequency drift. However, only the spin-plane component of the air drag acceleration vector is modulated; the component normal to the spin-plane (parallel to the spin axis) is not affected by the spin. This, of course, is independent of the orientation of the accelerometer sensing axes within the sphere.

### 2.1 Z-axis Relay

It has proven convenient to orient the accelerometer so that one of its sensing axes is normal to the spin plane thus placing the other two axes in the spin plane. In this manner two of the transducer amplifiers (X- and Y-axes) can be a.c. types having a narrow band-pass response centered on the spin frequency. The third amplifier, that for the Z-axis which must process the unmodulated acceleration component, necessarily must have a good low frequency response. This amplifier is therefore susceptible to the off-set drift inherent in d.c. amplifiers. This problem has been partially solved by the use of low-drift input semiconductor devices for the Z-axis amplifier so that off-set due to

drift is not apparent in the two lower gain ranges.

The state-of-the-art technique used to solve the problem of drift in d.c. amplifiers is to periodically remove the input signal voltage to allow the drift to be measured. Amplifiers of this type (chopper amplifiers) have been implemented during this program using semiconductor switching but were not suitable because of the lowered input impedance caused by the switch device leakage.

In the densitometer application the drift observed in the most sensitive range of the amplifier is slow as compared to the flight time interval corresponding to the time a particular channel is active. This fact suggested that the input switching could be accomplished by the use of a relay, one having a high open circuit leakage impedance, implemented so that only one closure would be programmed to occur, and this just preceding the time of high sensitivity operation. It should be emphasized that relay switching cannot be used in this application to chop the signal in the conventional manner because the mechanical transient acceleration due to the relay armature would cause unacceptable noise interference. This relay was incorporated into the Z-axis system and was caused to close at the time of uncaging. It was programmed to stay closed during the approximately seven-second mechanical transient (ringing) period of the transducer, thus removing the transient charge of the bimorph in addition to establishing the zero reference.

Flight data has confirmed that this system functions as anticipated. Flight data analysis suggests that an additional closure should be programmed to occur at apogee thus reestablishing the zero reference for the high sensitivity Z-axis down-leg data.

## 2.2 Z-axis Roll-off Compensation and Calibration

As shown in Figure 1 the electrical equivalent of the piezoelectric bimorph transducer is inherently a voltage generator connected to a series capacitance which in turn connects to the input resistor of the amplifier. Thus, it is seen that as the signal frequency decreases the attenuation increases by 6 db per octave and the transducer will not pass a steady-state voltage to the amplifier input. This is not an important constraint with regard to the X- and Y-axis amplifiers because the information involving these axes is carried on the sphere spin frequency (5-6 Hz). However, because the Z-axis data is not spin modulated and even though the Z-axis drag acceleration signal is not steady-state but is an exponentially-varying function, the signal attenuation due to the inherent RC coupling of the bimorph must be considered.

The loop equation for the input circuit of Figure 1 is

$$E = \frac{1}{C}\int i\,dt + Ri$$

and since $V = Ri$

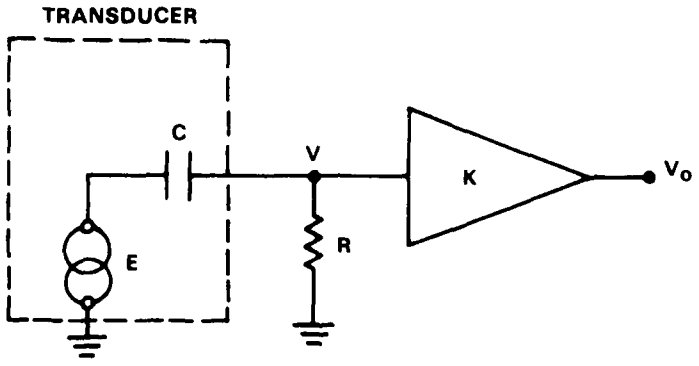


**Transducer Equivalent Circuit**

FIGURE 1.

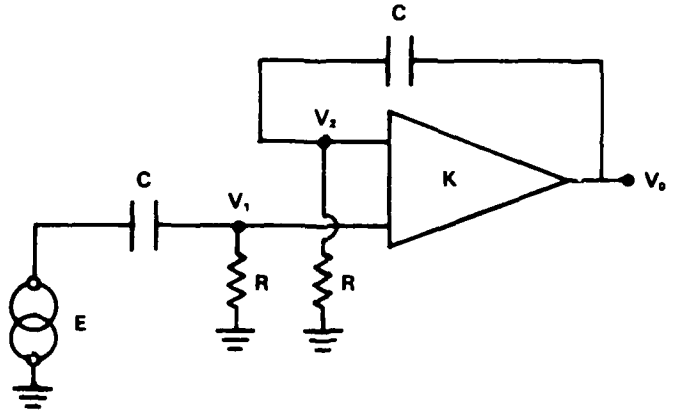


**Response Compensation Circuit**

FIGURE 2.

$$E = \frac{1}{RC}\int V dt + V \tag{1}$$

and because $V_0 = KV$

$$E = \frac{1}{K}\left[\frac{1}{RC}\int V_0 dt + V_0\right] \tag{2}$$

It is seen from the above that the circuit will pass any time function with minimum distortion provided that

$$\frac{1}{RC}\int V_0 dt << V_0$$

The first term in Equation 2 can be considered as an error in the analog signal. To minimize this error the RC product should be made as high as practicable.

The state-of-the-art technique used to correct for the attenuation produced by the RC coupling of Figure 1 is to use an operational amplifier with an identical RC circuit in the feedback path as shown in Figure 2. For this circuit one obtains two equations, in the form of Equation 1, for the input and feedback circuits:

$$E = \frac{1}{RC}\int V_1 dt + V_1 \tag{3}$$

$$V_0 = \frac{1}{RC}\int V_2 dt + V_2 \tag{4}$$

and for the differential amplifier portion of the circuit

$$V_0 = K(V_1 - V_2) \tag{5}$$

If the amplifier gain K is very high, as is usual for the operational-type amplifier, the quantity $(V_1 - V_2)$ is very small for any $V_0$ within its dynamic range. Thus, $V_1 \approx V_2$.

From Equations 3 and 4

$$V_1 = E - \frac{1}{RC}\int V_1 dt$$

$$V_2 = V_0 - \frac{1}{RC}\int V_2 dt$$

Substitution of these equations into Equation 5 gives

$$V_0 = K\left(E - \frac{1}{RC}\int V_1 dt - V_0 + \frac{1}{RC}\int V_2 dt\right)$$

and since $V_1 \approx V_2$

$$V_0 = K(E - V_0) \quad \text{or} \quad E = \left(\frac{1}{K} + 1\right)V_0 \qquad (6)$$

Comparison of Equation 6 with Equation 2 reveals that the error term in Equation 2 has been cancelled by the use of the feedback circuit.

The input circuit of Figure 2 can be considered to be a signal differentiator while the amplifier with its feedback circuit can be considered to be a signal integrator. For low-signal-level applications where the integration time interval is long such as with the Z-axis amplifier it is important that input off-set voltage be very small and that provision be made to periodically rezero the amplifier by discharging the capacitance to remove the

error caused by the integrated off-set voltage. Considerable time was expended in the examination of this circuit for possible use in the Z-axis chain. It was found that the error introduced by the integrated input off-set voltage exceeded the error due to the first term of Equation 2 when compared to the simple amplifier with a high input RC product.

It is seen from Equation 2 that for any RC product the true analog voltage E can be recovered by adding the quotient of the time integral of the output voltage and time constant to the output voltage by means of a computer. Since the output voltage is telemetered, this operation can be done with a general purpose computer on the ground. In this manner the flight amplifier requirement is made simple and straightforward enhancing system accuracy and reliability.

Because the down-leg air-drag acceleration analog voltage time function is closely approximated by the exponential

$$E = Ae^{t/T} \tag{7}$$

the transient response to this forcing function of the transducer equivalent circuit Figure 1 is given by combining Equations 2 and 7 to yield

$$Ae^{t/T} = \frac{1}{K}\left[\frac{1}{RC}\int V_0 dt + V_0\right]. \tag{8}$$

Distortionless amplification of the input function requires that the output be of the form

$$V = Be^{t/T}.$$

Substitution of this function into Equation 8 gives the solution

$$Ae^{t/T} = \frac{B}{K}\left[\frac{T}{RC}\, e^{t/T} + e^{t/T}\right]$$

from which

$$A = \frac{B}{K}\left[\frac{T}{RC} + 1\right]. \qquad (9)$$

It is seen, therefore, that the circuit as shown in Figure 1 will amplify a function such as described by Equation 7 without introducing distortion.

It should be pointed out that the above analysis pertains only to amplifier systems having a single time constant such as is the case with the nutation sensor amplifier. Reference to Equation 9 shows that it is possible to calculate the coefficient A and thus determine the desired input analog Equation 7. The constants B and T are readily determined from the flight data while K and RC are known circuit parameters.

## 2.3 Special-purpose Function Generator

Because of the necessity for the notching-out of the interfering nutational acceleration voltage, which is nominally at a frequency of 0.9 Hz, a twin-T filter is placed in the input circuit immediately after the Z-axis transducer. This complicates the input circuit in that it has more than

one RC time constant. It was for this reason that a special function generator was designed and fabricated. This instrument is capable of generating functions such as Equation 7 with the additional feature that anomalies encountered in flight may be simulated. This generator was then used to test the Z-axis amplifier chain to determine amplifier fidelity for functions closely representing those experienced in flight. Figure 3 depicts the test circuit used in these tests. As is apparent in the figure, the input voltage function was fed into two parallel paths: one through the amplifier under test and the other through purely a resistive network. The two outputs were compared by means of an adding circuit. If the amplifier produces the same function as the resistor network the output of the adding circuit will remain at zero. Any distortion produced by the amplifier will cause the output of the adding circuit to depart from zero. The results of these experiments are shown in Figure 4. The anomalous function used in these tests is exaggerated as compared to functions observed during flight but it is used to illustrate a worst-case condition. This function generator is presently being used to determine the Z-axis amplifier gain factors.

## 2.4 Redesigned Z-axis Amplifier

The distortion observable in the data presented in Figure 4 is largely due to the additional RC time constants necessarily introduced into the Z-axis amplifier chain by

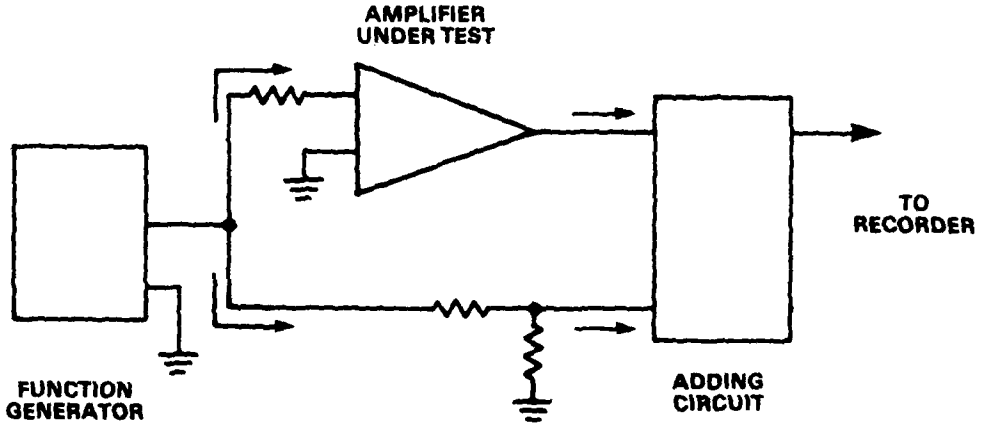


**Z-axis Amplifier Response Test Circuit**

FIGURE 3.

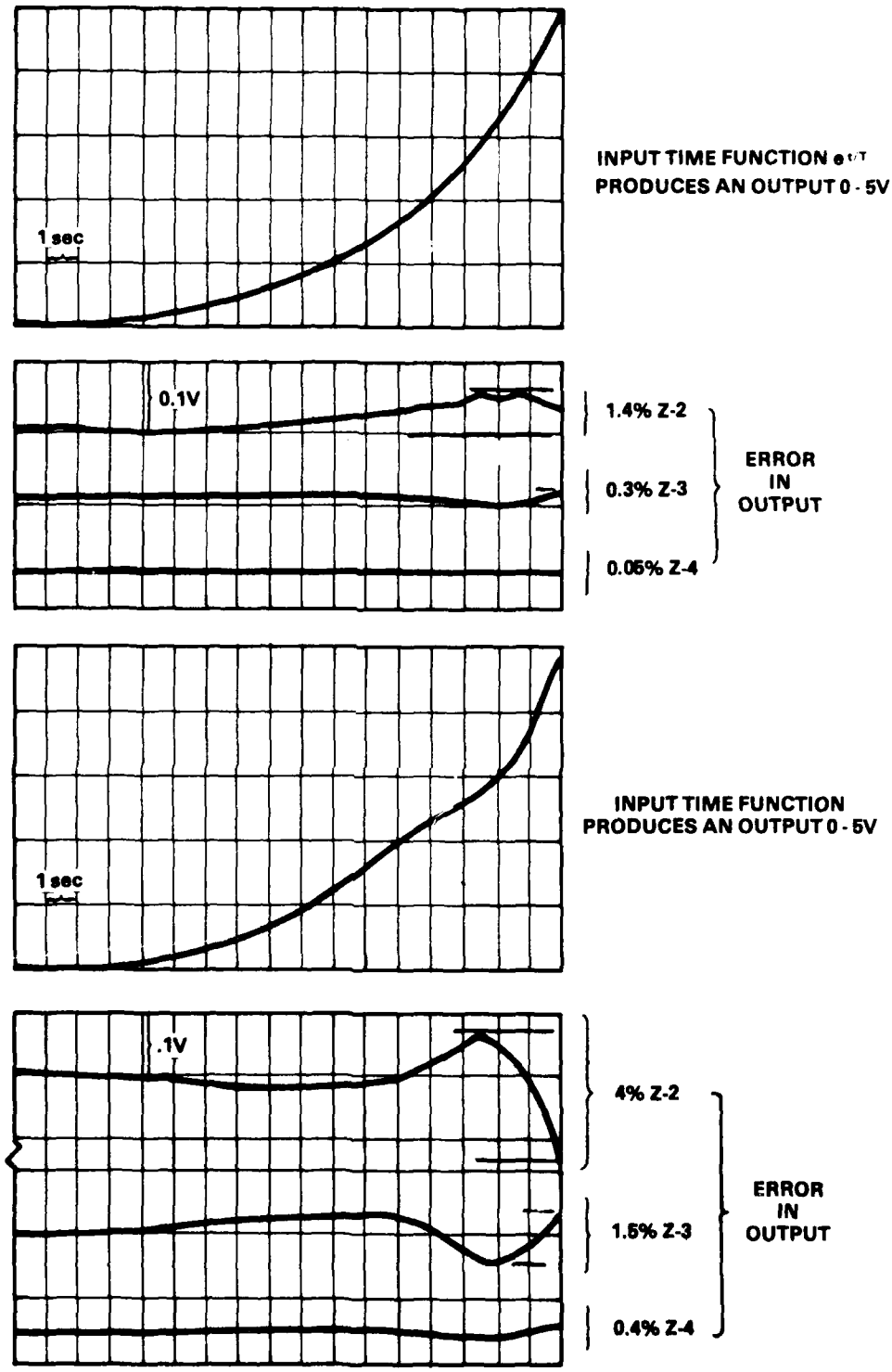


**Z-axis Amplifier Response**

FIGURE 4.

the twin-T notch filters used to remove nutational interference. The Z-axis amplifier chain, comprised of four amplifiers in series, originally was designed with the following filters:

| | |
|---|---|
| Z-1 | 4 cascaded twin-T |
| Z-2 | 3 cascaded twin-T |
| Z-3 | 1 twin-T |
| Z-4 | 1 twin-T |

Data analysis of the flight records from four previous flights revealed that the nutational acceleration interference was consistently small and of such amplitudes that the degree of filtering originally deemed necessary was not warranted. A new Z-axis chain was designed retaining only one notch filter as shown in Figure 5. Flight experience has verified the merit of this new system in that the small amount of nutational interference appearing in the outputs can be easily removed by computer processing on the ground.

Additionally, previous flight experience has shown that the high sensitivity (Z-1) data was unusable because of the long duration transient caused by the uncaging shock. This effect would be minimized by the Z-axis relay, described above, which was recently incorporated into the Z-axis amplifier front end. However, since Z-axis information is used only to determine aspect and because aspect is conserved due to spin momentum, it has been proven that the high sensitivity data is not needed, and this TM channel is now being used to telemeter the sphere internal temperature.

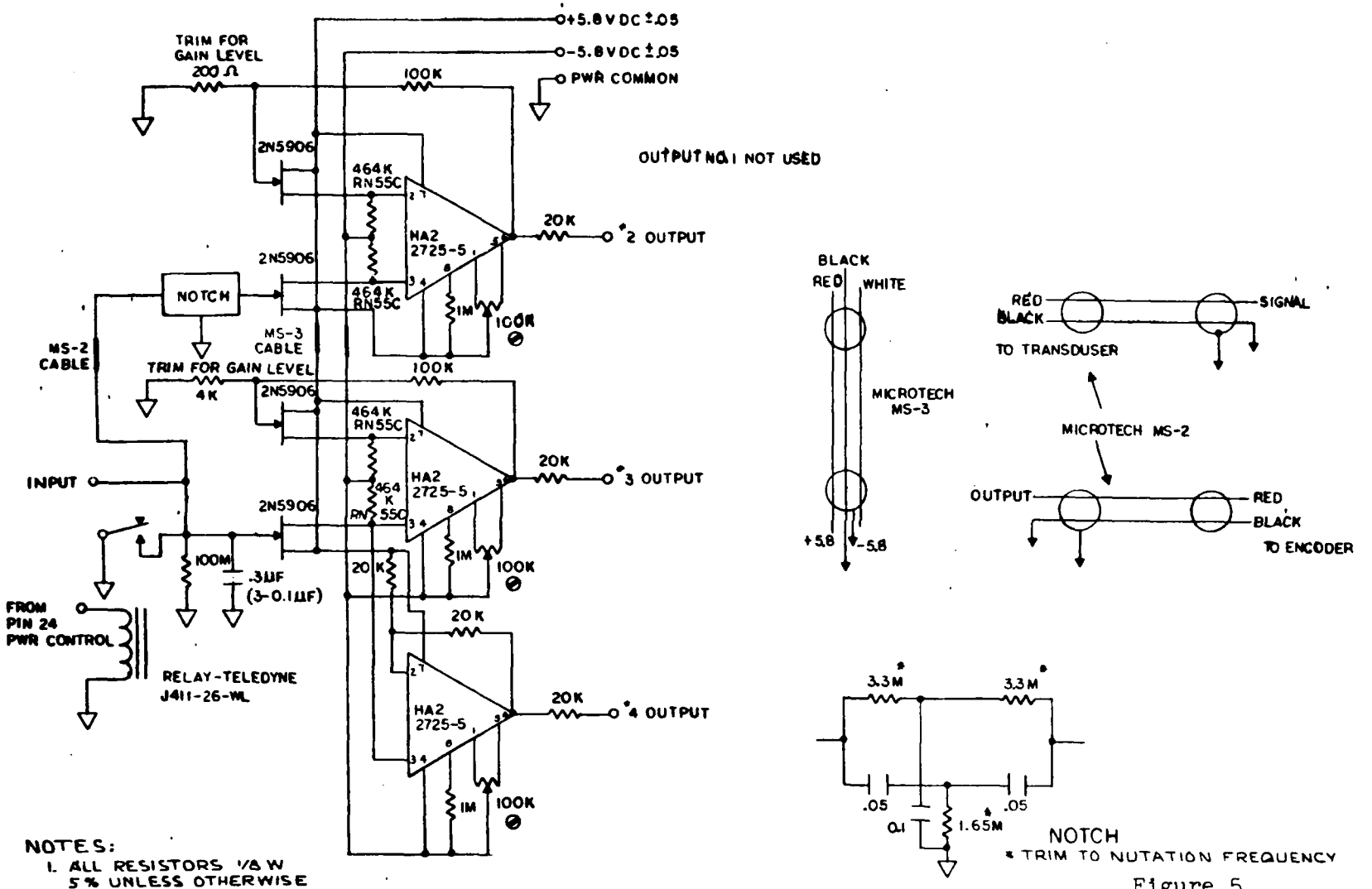


NOTES:

1. ALL RESISTORS 1/8 W 5% UNLESS OTHERWISE SPECIFIED.
2. ALL CAPACITORS CORNING K 10% UNLESS OTHERWISE SPECIFIED.

Figure 5

| PART NO. | NO REQ'D | DESCRIPTION | MATLS & SPECIFICATIONS |
|---|---|---|---|

| REV LET | DESCRIPTION | CHK'R BY & DATE | ENG APPR |
|---|---|---|---|

DO NOT SCALE FOR CONSTRUCTION

TOLERANCES UNLESS OTHERWISE SPECIFIED
FRACTIONAL ± 1/64 UP TO 24" ± 1/32 OVER 24" DECIMAL .X ± .01 .XX ± .005 .XXX ± .002 ANGULAR DEGREES ± 1/2° MINUTES ± 5' CONCENTRICITY .005 TIR FINISH 63 RMS MICRO IN

| APPROVED | DATE |
|---|---|
| DESIGN ENG | |
| PROJ ENG | 4 DEC 79 |
| MFG | |
| PART REQ'D BY | |
| MFG BY | |

ACCUMETRICS CORPORATION
344 RINDGE AVENUE
CAMBRIDGE, MASS 02140
617 868-1142

TITLE: SCHEMATIC DIAGRAM Z AXIS AMPLIFIER

REF DWG

PROJ

| DR BY | DATE | CH'K BY | DATE |
|---|---|---|---|
| | | | 12-1-79 |

SCALE | C | 100115

5

## 2.5 Temperature Monitoring

The internal temperature data was formerly multiplexed with the nutation data in a single TM channel. The temperature data lies in a very narrow frequency band centered around zero frequency while the nutation data lies in a similar narrow band centered around 0.9 Hz. This has enabled the simple addition of these data for telemetry in a single channel. Thus, the temperature appeared as an off-set in the zero crossing of the nutation sinewave. Because of the addition of these voltages the total dynamic range of the channel had to be apportioned. The apportionment was made to favor the nutation sensor because this sensor being an accelerometer provides, as a bonus, additional very low altitude drag data. The temperature scaling in this channel therefore was compressed which made it inaccurate. For this reason the internal temperature measuring circuit was redesigned to expand its scaling and this data was placed in the TM channel formerly used for the Z-1 data. Figure 6 is a schematic of the new temperature monitor system.

## 2.6 Sensitivity Range Overlap

In order to cover the very considerable dynamic range requirement of $10^7$ for the sphere system the amplifier outputs of the X and Y axes are each placed in four PCM telemetry channels with each channel covering 1.75 decades of the total range. Formerly, the X and Y range division was identical: the channel in the X measurement covering the same

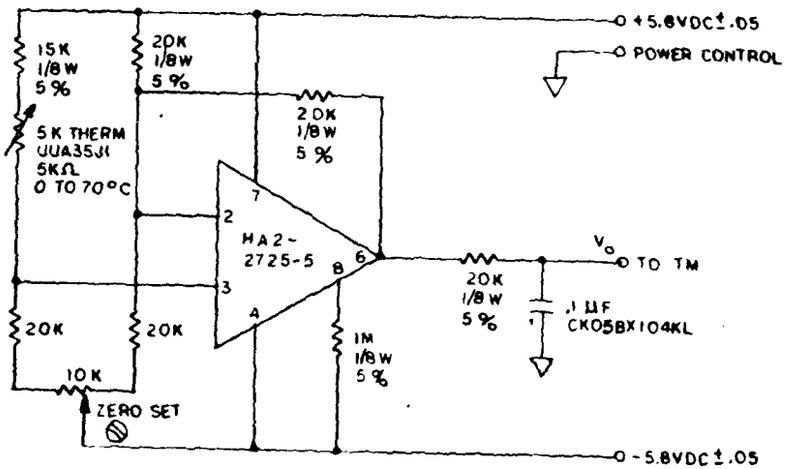


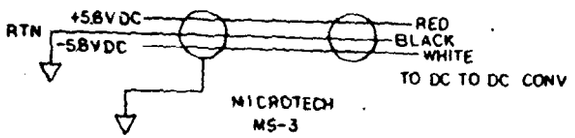


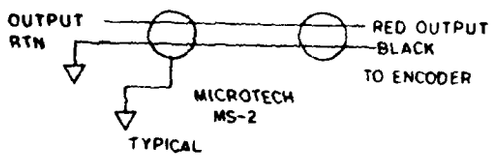


| $V_o$ | TEMP | |
|---|---|---|
| MV | °F | °C |
| -800 | 60 | 15.6 |
| -550 | 65 | 18.3 |
| -100 | 70 | 21.1 |
| 0 | 72 | 22.2 |
| 240 | 76 | 24.4 |
| 450 | 80 | 26.7 |
| 650 | 85 | 29.4 |
| 1200 | 100 | 37.8 |

SEE CURVE FOR EXTENDED RANGE

Figure 6

| PART NO. | NO. REQ'D | DESCRIPTION | MATERIAL & MFG. RATINGS |
|---|---|---|---|
| APPROVED | DATE | | |
| DESIGN ENG | | | |
| PROJ. ENG | | | |
| MFG | | | |
| PART REQ'D BY | | | |
| MFG. BY | | | |

TITLE: TEMPERATURE MONITOR CIRCUIT

REF DWG

PROJ

DR BY | DATE | CHK'D BY | DATE

SCALE | C | 100113

| REV LET | DESCRIPTION | CHK'D BY & DATE | ENG APPR. |
|---|---|---|---|

DO NOT SCALE FOR CONSTRUCTION

TOLERANCES UNLESS OTHERWISE SPECIFIED

| FRACTIONAL | DECIMAL | ANGULAR |
|---|---|---|
| UP TO 24" ± 64 | XX ± .01 | DEGREES ± 2° |
| OVER 24" ± 32 | XXX ± .005 | MINUTES ± 5' |

FINISH 63 RMS MICROIN | CONCENTRICITY .005 T.I.R.

ACCUTRONICS CORPORATION
344 RINDGE AVENUE
CAMBRIDGE MASS 02140
617 868 1182

time interval as the corresponding channel in the Y measurement.

Because the PCM data accuracy inherently degrades at low signal levels, the X- and Y-axis amplifier gain levels have been changed to stagger the channels so that when the output of one axis is at the minimum end of its range in a particular channel the output of the other axis is at approximately one-third of its range in the corresponding channel. Thus, with the aid of aspect information it is possible to obtain greater precision in data reduction during the intervals when one axis is nearing its minimum level by referring to the other axis and using its higher level, and hence, more accurate data.

## III. SENSITIVITY AND NATURAL FREQUENCY CORRECTIONS

### 3.0 General

Study effort expended on this program has resulted in the refinement of accelerometer calibration data through a more precise determination of the transducer natural frequencies. These studies revealed that the sea-level gravity field affects by a small fixed amount the natural frequency as measured in the laboratory, and the spin-induced radial centrifugal acceleration field affects, again by a small fixed amount, the natural frequency during flight. The results of analysis have yielded straight-forward formulae to facilitate the proper corrections to obtain the true transducer natural frequency.

The voltage generated by the piezoelectric transducer is given by

$$V = \frac{KA}{\omega_n^2 \left\{ \left[ 1 - \left( \frac{\omega}{\omega_n} \right)^2 \right]^2 + \left[ 2\zeta \frac{\omega}{\omega_n} \right]^2 \right\}^{\frac{1}{2}}} \qquad (1)$$

Because its damping ratio $\zeta$ is small ($5 \times 10^{-3}$) the above equation simplifies to

$$V = \frac{KA}{\omega_n^2 \left[ 1 - \left( \frac{\omega}{\omega_n} \right)^2 \right]} \qquad (2)$$

The transducer is calibrated by measuring its output voltage while under excitation by a known sine-wave acceleration. Its natural frequency is determined by measurement

of its free oscillation after shock excitation. The constant K is then calculated from Equation 2. Because the flight acceleration frequency and flight natural frequency are different from the corresponding test quantities the same equation must be used to obtain the air-drag acceleration corresponding to the transducer voltage derived from TM records.

## 3.1 Gravity Correction

The transducer natural frequency is modified at sea level by an additional restoring force due to gravity arising out of its pendulous shape and its vertical orientation during calibration. In general, the dynamical force equation for the lightly damped spring-mass system representing the transducer is given by

$$m\ddot{x} = -Kx \tag{3}$$

The additional pendulous restoring force for small deflections is mgx/l so that at sea level the transducer dynamical equation is

$$m\ddot{x} = -Kx - m\frac{g}{l}x$$

or

$$\ddot{x} + \left(\frac{K}{m} + \frac{g}{l}\right)x = 0$$

from which the sea-level natural frequency is seen to be

$$\omega_{nT} = \left(\frac{K}{m} + \frac{g}{l}\right)^{\frac{1}{2}} \tag{4}$$

This is the quantity measured in the laboratory during transducer calibration. Reducing g to zero in Equation 4 one obtains its free-fall natural frequency

$$\omega_n = \left(\frac{K}{m}\right)^{\frac{1}{2}} \tag{5}$$

and by substitution of Equation 5 into 4 gives the correction formula

$$\omega_n = \left(\omega_{nT}^2 - \frac{g}{l}\right)^{\frac{1}{2}} \tag{6}$$

where g is the local acceleration due to gravity and l is the length of the transducer measured from the base of the bimorph to the load mass-center.

## 3.2 Spin Correction

Because the sphere is spin stabilized the natural frequencies of the spin-plane transducers are modified during flight by the negative restoring force caused by the centrifugal acceleration $mR\omega^2$. Reference to Figure 7 shows that the component of this force along the line of motion freedom is given by

$$F_c = mR\omega_s^2\cos\theta.$$

Also from the figure

$$X = R\cos\theta$$

so that

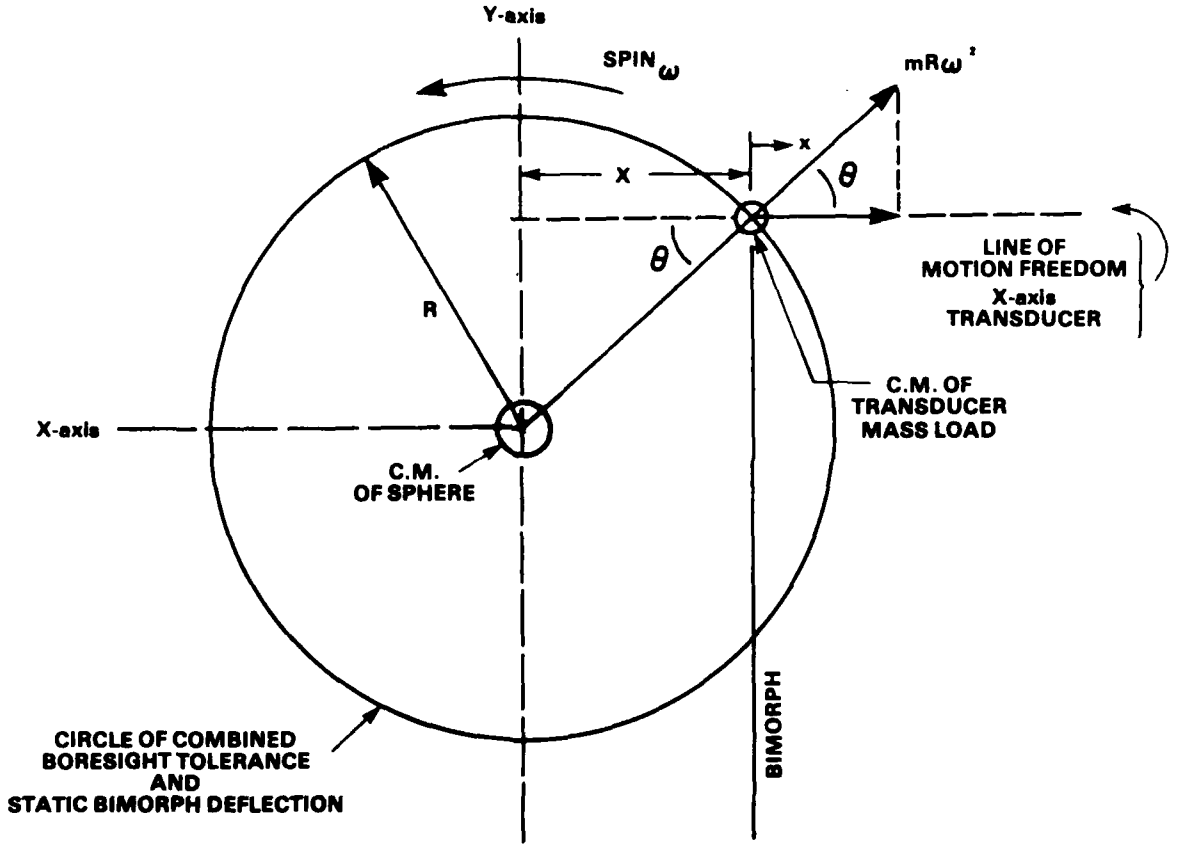


**Transducer Bore-sight Geometry**

FIGURE 7.

$$F_c = mX\omega_s^2 \tag{7}$$

In the absence of air-drag acceleration this force is opposed by the spring force of the transducer

$$mX\omega_s^2 - Kd = 0$$

where d is the deflection of the transducer. The distance X in the figure is the sum of the error T in mass-center bore-sighting and the deflection d, hence

$$d = X - T$$

so that the equilibrium force equation is

$$mX\omega_s^2 - K(X - T) = 0$$

or

$$\omega_s^2 - \omega_n^2\left(1 - \frac{T}{X}\right) = 0$$

from which

$$X = \frac{T}{1 - \left(\frac{\omega_s}{\omega_n}\right)^2} \tag{8}$$

which defines the equilibrium position of the transducer mass-center in terms of the error in bore-sighting of the instrument. The dynamical equation, neglecting the very small damping term describing the motion of the transducer is referenced to the equilibrium position X and therefore

is in terms of x (see Figure 7):

$$m\ddot{x} + Kx - m\omega_s{}^2 x = mA\sin\omega_s t$$

or

$$\ddot{x} + \left(\frac{K}{m} - \omega_s{}^2\right)x = A\sin\omega_s t \qquad (9)$$

from which the coefficient of x gives the natural frequency for the spinning system:

$$\omega_{ns} = \left(\omega_n{}^2 - \omega_s{}^2\right)^{\frac{1}{2}} \qquad (10)$$

3.3 Overall Sensitivity Correction

As mentioned above, the constant K in Equation 2 is obtained from laboratory measurements. The test quantities of frequencies and amplitudes are substituted into Equation 2 to give

$$K = \omega_{nT}{}^2\left[1 - \left(\frac{\omega_T}{\omega_{nT}}\right)^2\right]\frac{V_T}{A_T} \qquad (11)$$

Again, by the use of Equation 2 the flight transducer sensitivity is then given by

$$\frac{V}{A} = \frac{K}{\omega_{ns}{}^2\left[1 - \left(\frac{\omega_s}{\omega_{ns}}\right)^2\right]} \qquad (12)$$

By combining Equations 11 and 12 the overall sensitivity correction formula is obtained:

$$\frac{V}{A} = \frac{V_T}{A_T} \frac{\omega_{nT}^2 - \omega_T^2}{\omega_{ns}^2 - \omega_s^2} \qquad (13)$$

# IV. CALIBRATION BENCH

## 4.0 General

As described in detail in Report No. AFGL-TR-78-0058 the accelerometer transducers are calibrated by the use of a sine-wave displacement generator which produces a horizontal motion of the base of the transducer. The amplitude of this motion is measured by the use of a calibrated microscope and is the most critical measurement to perform in the calibration process. Because the accelerometer is an inertial device it is important that a base be provided for the microscope that is essentially devoid of dynamical acceleration. It was discovered that the test bench formerly used for this task was affected by the reaction of the electromagnetic displacement generator causing an error in the measurement of the true inertially referenced displacement of the transducer.

## 4.1 Bench Design

A new calibration bench, shown in Figure 8, has been designed and fabricated and is now in use. The bench is of steel reinforced 4x4 wood dimension stock having a heavy steel top. To reduce the susceptibility of the bench to seismic noise (traffic, wind, etc.) it has been located over the portion of the laboratory floor lying directly above the concrete foundation support wall.

Included in this effort was the redesign and fabrication of the suspension system which supports the transducer

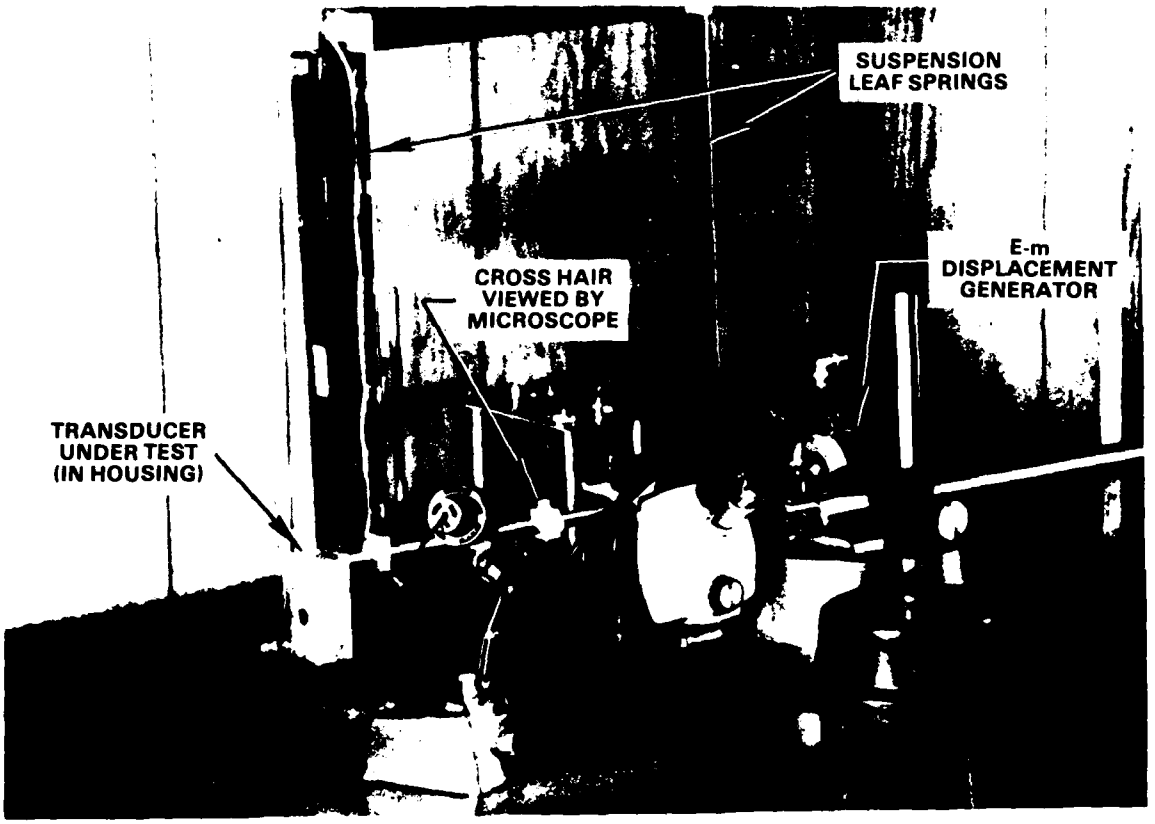


**Transducer Test Bench**

FIGURE 8.

under test. The salient improvement here was the lengthening of the vertical suspension leaf springs from six to eighteen inches, thus, proportionately reducing the curvature of the locus of the transducer movement to enable the production of a more true linear displacement.

# V. SQUIB INITIATION CIRCUIT

## 5.0 General

As discussed in Report No. AFGL-TR-0187, Part 6.2, from data analysis of the records of previous flights there was evidence that the DM25J5 uncaging dimple motor squibs were generating actuation pressures in excess of design levels. Tests in the laboratory indicated that approximately 10% of the test samples ruptured their cases resulting in a high level shock and in the scattering of debris. Because these squibs were being initiated according to the manufacturer's specifications a call was made to their laboratory for consultation. The manufacturer verified the rupture problem from other independent tests and determined that the cause was due to excessive initiation energy. They recommended the use of the capacitor dump circuit shown in Figure 9. This circuit, as opposed to the direct battery initiation circuit then being used in the sphere system, limits the energy level to 7,500 ergs.

## 5.1 Capacitor Dump Circuit

The circuit shown in Figure 9 was incorporated into the sphere system and was thoroughly tested both in the laboratory and in the field during prelaunch preparations. Of the 12 squibs tested all performed satisfactorily producing the required actuation without rupture. However, in two successive flights, analysis of the TM data revealed that the squibs did not initiate and the instrument did not uncage.

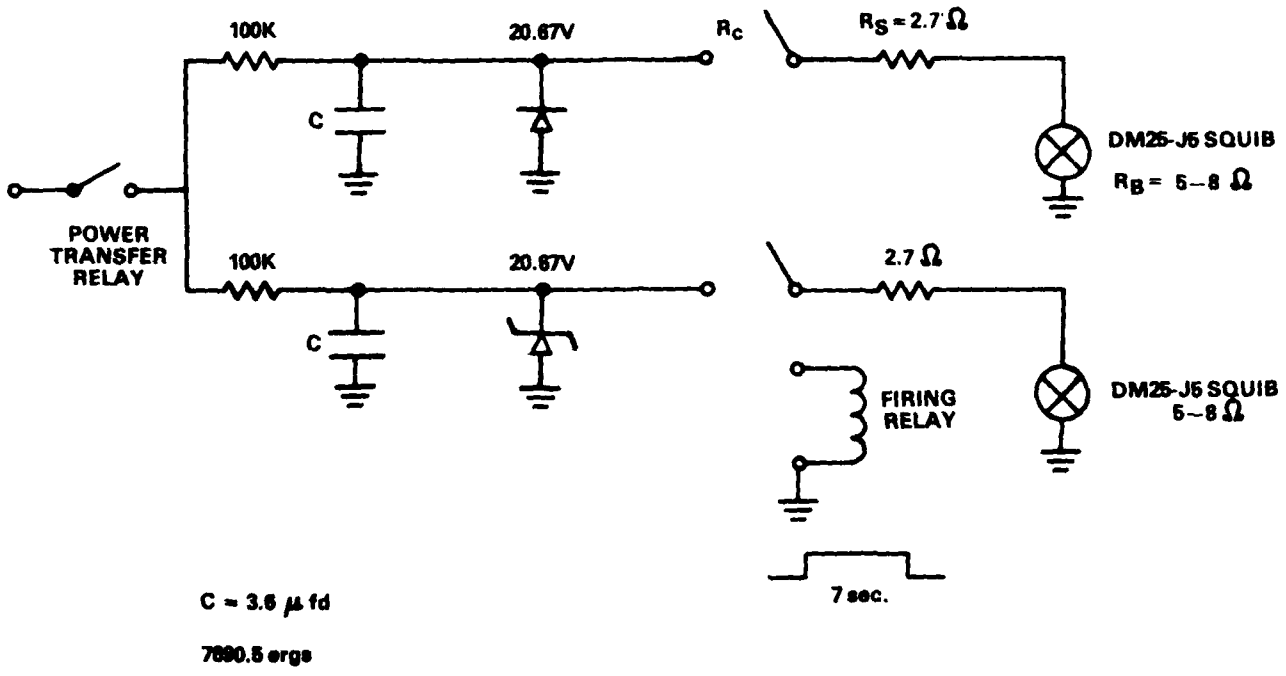


**Capacitor Dump Circuit**

FIGURE 9.

Considerable effort was expended in the study to determine the cause of this malfunction. It has been concluded that because the electrical current transient in the recommended circuit is of such small duration (33 μsec) that unless the relay switching produces a nearly instantaneous resistance change from infinity to near zero a meaningful fraction of the energy will be dissipated in heat at the relay contacts. This energy, because of the limiting feature of the circuit, subtracts from that available for squib initiation. This is apparent from the following analysis.

In reference to Figure 9 the energy in the squib circuit upon closure of the firing relay is

$$W = \int i^2 (R_c + R_s + R_b) dt.$$

The current is given by

$$i = \frac{V_0}{R_T} e^{-t/R_T c}$$

where $R_T = R_c + R_s + R_b$ so that

$$W = \int \frac{V_0^2}{R_T^2} (R_c + R_s + R_b) e^{-2t/R_T c} \, dt$$

$$= \frac{1}{2} C V_0^2 \frac{R_c + R_s + R_b}{R_T} e^{-2t/R_T c}$$

It is seen that the energy is at a level $1/2CV_0^2$ at time equal zero and is fractionally apportioned directly

as the fractional resistance apportionment. Also, it is seen that this energy pulse is essentially depleted at $T = R_T C$, which is equal to 33 microseconds for the circuit in the figure if the contact resistance is neglected.

A switch contact, especially if operating at light pressure, does not instantaneously change its resistance in ohms from infinity to zero but takes a finite time, in this case a fraction of its 2-millisecond operating time, to execute a wiping motion to establish its final low-resistance contact position. During the wiping action the resistance varies from infinity through all resistance values to a low value of approximately 0.1 ohms. This action would entail a time duration of 20 microseconds allowing a wiping time of 1% of the relay operating time.

It is reasonable to conclude therefore that during the larger part of the energy pulse transient the fractional resistance of the relay contact was large compared to that of the squib bridge-wire resistance and a large fraction of the energy available for squib initiation was dissipated instead in contact heat. It is felt that the centrifugal acceleration on the relay armature caused by spin during flight adversely affected contact pressure aggravating this effect so that the malfunction was observed only during flight and not during the laboratory and prelaunch field tests. Further tests in the laboratory proved that if the dimple motor squib initiated by the simple battery

and relay circuit is properly surrounded by a heat-sinking sleeve, initiation can be achieved without explosive rupture. Of 20 samples tested no malfunction was observed even though the initiation voltage was maintained for periods longer than the seven-second discrete pulse used in flight.

## 5.2 Redesigned Initiation System

In all former cases when squib rupture did occur it was observed that the operation of uncaging performed satisfactorily in a mechanical sense but the accompanying flying debris of the rupture created a hazard to the nearby instrument components. In addition, the shock of the rupture caused a long-duration ringing transient in the transducer outputs which reduced the useful up-leg data. In view of the low probability of squib rupture using the heat-sink technique it was decided that this method be incorporated into the system using the former nonlimiting relay-battery initiation circuit. Heat sinking was obtained by redesigning the squib-holder bushings to fit more closely to the outer diameter of the squib housing. These bushings are now machined from stainless steel and lengthened to enable the effective captivation of debris in the event of squib rupture. In this low-probability case the system would perform satisfactorily except that the amount of useful up-leg data would be reduced.

# VI. FLIGHT TESTING

## 6.0 General

Field services were provided for the payload preparation and launching of three densitometer systems: two at KMR, Kwajalein, M.I., and one at Red Lake, Ontario, Canada. A fourth system was prepared for launch at WSMR, New Mexico but was not launched because of a malfunction in the prime rocket.

## 6.1 KMR Field Trip

Densitometer Systems AC-7 and AC-9 were flown at KMR on 4 April 1978. The launch of AC-7 was unsuccessful due to a malfunction in the Nike-Hydac second stage ignition system. The launch of AC-9 was successful in that programmed altitude and clean payload separation were achieved. Only limited scientific data were obtained, however, because of loss of ignition of the squibs used to uncage the accelerometer. Further examination of the flight data for the first launch revealed that the same malfunction occurred in the performance of AC-7. The causes and corrections for the squib malfunction are discussed in detail in Part V of this report.



## 6.2 WSMR Field Trip

Densitometer System AC-8 was prepared for launch scheduled for flight on 15 May 1978 in support of DMSP. Because of a malfunction in the primary vehicle (Aerobee

170), which preceded the intended launch time of sphere AC-8, the program was cancelled and sphere AC-8 was returned to AFGL to await rescheduling.

## 6.3 Red Lake Field Trip

Densitometer System AC-10 was flown at Red Lake, Ontario, Canada on 26 February 1979 as part of the 1979 Solar Eclipse Program. All systems performed satisfactorily during pre-launch tests and during the flight. The flight records obtained were clean and free from anomalies insofar as hardware performance is concerned. Scientific data reduction has not been completed at the time of this writing.